ELSEVIER

Contents lists available at ScienceDirect

## Additive Manufacturing

journal homepage: www.elsevier.com/locate/addma

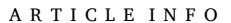


### Research paper

# Complex ink flow mechanisms in micro-direct-ink-writing and their implications on flow rate control

Kevin T. Estelle a, B. Arda Gozen a,b,\*

- <sup>a</sup> Washington State University, School of Mechanical and Materials Engineering, USA
- <sup>b</sup> Washington State University, Voiland School of Chemical and Bioengineering, USA



Keywords: 3D printing Micro extrusion Rheology Wall slip Non-Newtonian Water-based ink

### ABSTRACT

Despite its simplicity, low cost, and ability to process a wide range of materials, direct-ink-writing (DIW) is an additive manufacturing process with low resolution and accuracy, in the multiple hundred microns to millimeter range. One of the main sources for this issue is the difficulty with accurately controlling ink flow rate at smaller size scales. Towards addressing this limitation, this paper elucidates complex ink flow mechanisms that renders flow rate control difficult and explores printing implementations to increase flow rate accuracy in direct-inkwriting at the micro scale. To this end, a DIW system utilizing hybrid pressure and velocity-controlled extrusion is used to obtain pressure-flow rate relationships for a water-based sodium carboxymethyl cellulose (NaCMC) solution ink, as a function of printing nozzle diameter (510–100  $\mu m$ ). These studies showed that the transient response of piston velocity-controlled extrusion significantly slows down with decreasing nozzle diameter. For pressure-controlled extrusion, the wall slip increases with decreasing nozzle diameter and the constant slip velocity assumption no longer holds as nozzle size decreases below a certain diameter. To contextualize the influence of such behavior on flow rate accuracy, temperature-controlled parallel plate rheometry was performed on the inks and rheological ink models were accordingly determined. It was shown that the associated flow rate predictions under predicted flow rates due to lack of wall-slip consideration, particularly for smaller nozzle sizes. Lastly, an iterative pressure-controlled DIW implementation was explored to address the accuracy issues for micro-DIW. Our results indicated significant improvement in the transient response and flow rate accuracy for nozzle diameters as small as 100 µm using this approach compared to both of the conventional pressure and velocity control approaches.

### 1. Introduction

Direct-ink-writing (DIW) is an additive manufacturing method known for its ability to process a wide range of materials, its simplicity, and low cost. These attributes have led to it being a foundational method for emerging technologies such as bioprinting [1] and printed electronics [2]. One main avenue to further advance these technologies is to improve their printing resolution during micro-extrusion, which would increase final part accuracy and allow for further miniaturization of technologies. However, relatively low printing resolution is a current drawback for DIW as it has low dimensional accuracy due to difficulty with accurately controlling volume flow rate at smaller size scales [3]. Difficulty in controlling volume flow rate for micro-DIW can be attributed to many factors, such as ink heterogeneity and compressibility, non-ideal transient response during extrusion, complex ink behavior

such as wall slip [4,5] and temperature dependence of ink properties [6]. Some of these challenges have been shown to be exacerbated as size scale decreases, while the size-dependency of others require more research.

Besides the vexing ink behavior, the current state-of-the-art print head implementations commonly used for DIW lack robustness to adequately handle the level of uncontrollability in volume flow rate associated with extruding these inks (Fig. 1). Pneumatic systems use back pressure provided by compressed air to push a plunger through an ink-filled syringe and extrude the ink through a nozzle. To determine the correct input pressure associated for the desired volume flow rate, an indepth knowledge of the ink rheology and capillary flow mechanisms of the inks are required. Studies to date aiming to correlate input pressure with flow rate simplify these flow mechanisms to non-Newtonian flow with no wall slip, for which analytical relationships exist, provided that

E-mail address: arda.gozen@wsu.edu (B.A. Gozen).

<sup>\*</sup> Corresponding author.

# Positive Displacement: Velocity control Pneumatic System: Pressure control Motor Lead Screw Ink Nozzle

Fig. 1. Schematic of pressure- and velocity-controlled extrusion systems.

the ink rheology is well characterized [6,7]. However, it is also known that capillary flow mechanisms can be very complex and difficult to characterize due to wall slip effects, particularly for complex inks with various constituents [8] and when small nozzles are involved [9]. Another common DIW variation is a velocity-controlled system where an actuator drives a plunger-capped leadscrew at a set velocity through an ink-filled syringe in order to extrude ink through the nozzle. While this method can achieve desired volume flow rates, as the flow rate is dictated directly through the piston speed, it is still inadequate mainly because of ink compressibility causing undesirably long durations for the system to reach a steady-state where the flow rate near the piston is equal to that at the end of the nozzle [10]. In addition to these challenges, both approaches are open-loop implementations such that they are insensitive to fluctuations in the ink properties and associated variations of flow rate. There have been several recent efforts to establish closed-loop volume flow rate control schemes building off of these conventional printing schemes [7,11–14]. These methods have achieved volume flow rate control while processing materials with simple rheological properties (i.e., Newtonian or power-law) and/or millimeter scale nozzles for which the aforementioned complexities have minimal effect on the process outcome. It is evident that there is a lack of fundamental understanding of how these complex inks behave during micro-extrusion. This knowledge gap is a key factor limiting the ability to control volume flow rate and therefore printing accuracy and resolution.

Additionally, the absence of this understanding has brought to light that there are unexplored avenues for more advanced printing systems and the specific requirements for them to be able to handle the challenges of direct-ink-writing of complex inks at the micro scale. Understanding of the ink rheology and capillary flow mechanisms must be furthered before a suitable printing system can be developed. To this end, this paper elucidates the size-dependent non-Newtonian ink behavior during micro-extrusion that is limiting the state-of-the-art printing methods. Lastly, preliminary work, informed by the results presented on the development of a closed-loop scheme, aiming to achieve flow rate control which can address the challenges associated with micro-DIW processes is discussed.

### 2. Methods and materials

### 2.1. Materials

A water-based sodium carboxymethyl cellulose (NaCMC, Sigma Aldrich) solution was prepared and used as the ink at a concentration of 20% w/w and at a molecular weight of 90 kDa. To prepare the ink, 30 g of deionized water was placed in a glass container and then 6 g of NaCMC was added. The constituents were then combined with a mixer (Cole-Parmer Compact Digital Mixer System) for 12 h at 100 RPM. The ink was then stored in a closed glass jar at ambient temperature. Just before extrusion, the ink was syringed into a 5-cc gas-tight glass syringe, and then centrifuged (Nordson EFD ProcessMate<sup>TM</sup> 5000, PLC-012) for 10 min at 4000RPM to remove any air bubbles.

### 2.2. Rotational rheological characterization and predictive flow modelling

The ink rotational rheology was characterized using 25 mm-diameter parallel plate geometry on a strain-controlled rheometer (TA Instruments, ARES-G2) through temperature-controlled flow ramp experiments. In the flow ramp test, the ink behavior under increasing shear rates was characterized by varying the shear rate over 5 min from 1 to 100~1/s logarithmically. Specific emphasis was placed on the influence of possible slip between the material and the plates and the temperature sensitivity of the ink rheology. To investigate the former, the tests were repeated at gap heights of 0.333, and 0.25, and 0.166 mm and the produced data was used to perform the Mooney analysis [5], details of which are given in Supporting information S1.1. To investigate the temperature effect, each of the flow ramp experiments were run at three distinct constant temperature levels of 17, 20, and 23 °C. The stress vs strain rate data obtained at various temperatures was fitted with the Herschel-Bulkley fluid model given by [11]:

$$\tau = \tau_0 + k\dot{\gamma}^n \tag{1}$$

where  $\tau$  is the yield stress (Pa),  $\tau_0$  is the yield stress (Pa),  $\dot{\gamma}$  is the shear rate (1/s), k is the consistency index (Pa.s<sup>n</sup>), and n is the flow behavior index (dimensionless). Through this approach, we studied how these parameters vary with temperature. (see Table S1 in supporting information section S1.1).

### 2.3. Hybrid direct-ink-writing system

Extrusion experiments were carried out using a custom in-house built extrusion system as detailed in Fig. 2. A non-captive, leadscrew-based linear stepper motor (SMA-23SN-037062-3.25 V, Helix Linear) capped with a plunger acts as the printhead to regulate flow of ink from a glass syringe (SYR-GL5LL-S, New Era) to a pressure sensor (MFP Flow Plus, ElveFlow) and finally to a print nozzle. The motor is supported by the linear bearing assembly to prevent the leadscrew from rotating in place. The system is controlled through a Teensy (PJRC Teensy 4.1) microcontroller. The controller script is designed to operate in both constant velocity mode or a constant pressure mode, simply representing the two conventional printhead implementations of velocity-controlled and pressure-controlled, respectively. The constant velocity mode takes a velocity input and moves the piston axially in the positive or negative direction. The constant pressure mode utilizes a proportional derivative (PD) closed-loop pressure control using feedback from the pressure sensor as ink flows through it. The PD controller dictates the piston acceleration leading to the piston moving to achieve minimal error between the desired and measured pressures. The PD controller executes every 8 ms, and gain values of  $\ensuremath{K_p} = 0.005$  and  $\ensuremath{K_d} = 0.01$  were determined experimentally prior to all extrusion experiments. The experimentation process is controlled by a separate MATLAB code in serial communication with the microcontroller where desired pressure and PD gains can be edited real time. A microscope camera (Sentech STC

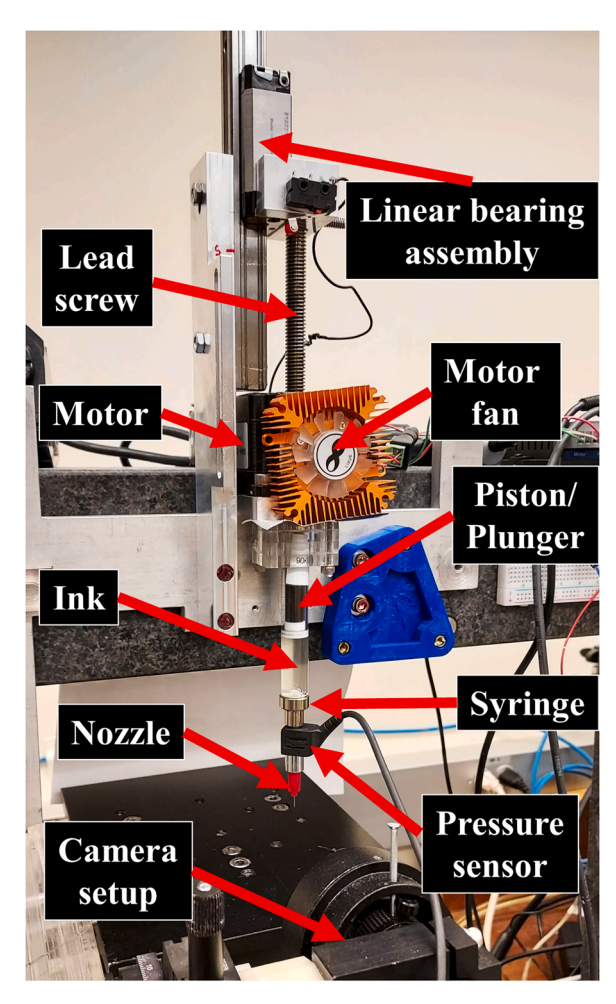


Fig. 2. Hybrid direct-ink-write system setup.

MCCM200U3V) with an in-house built vibration-dampening mount was integrated into the system to monitor the extrusion procedure visually.

### 2.4. Extrusion experiments

Two variations of experiments were conducted using the hybrid printhead to elucidate pressure-flow rate relationships during DIW with an emphasis on nozzle size dependence. Printing nozzles with 100, 150, 250, 330, and 510  $\mu m$  nominal inner diameters (Nordson 7018462, 7018424, 7018333, 7018302, 7005005, respectively) were used.

### 2.4.1. Transient behavior of the velocity-controlled approach

This experiment was carried out to observe the transient response of pressure during velocity-controlled ink extrusion for various nozzle sizes, where the target flow rate is dictated by the constant piston velocity such that  $v_{piston} = \frac{Q}{\pi R_{piston}^2}$  where Q is the desired volume flow rate and  $R_{piston}$  is the radius of the piston. Specifically, the system was run at a constant piston velocity while observing the rate of change of pressure towards the steady-state level. Pressure reaching steady state is a key indicator and requirement along with constant piston velocity for steady flow rate. Ink was extruded through nozzles of length 13 mm and inner diameters of 510, 330, 250, 150, and 100  $\mu$ m at a fixed piston velocity ranging from 4.71E-05–1.23E-03 mm/s. Two different experiments were carried out: (1) a constant piston velocity of 5E-04 mm/s was used across all nozzle sizes, and (2) a constant nozzle exit velocity of 0.5 mm/s was used for all nozzles, where  $v_{exit,nozzle} = \frac{Q}{\pi R_{nozzle}^2}$ . A piston velocity of 0.1 mm/s was set initially to prime the system by ensuring the pressure

sensor and nozzle were quickly filled with ink. Once the pressure reading began rising from the baseline pressure measured at the state where the ink completely fills the pressure sensor without flow, a velocity of -0.05 mm/s was set to retract the piston until pressure fell and read the baseline value again. The target velocity was then prescribed, and the system was allowed to run for 240 s as pressure was recorded.

### 2.4.2. Study of slip and end effects in flow behavior during ink extrusion

These experiments were carried out to generate the pressure vs flow rate data used to primarily study wall slip in a manner similar to the Mooney analysis performed during conventional capillary rheometry [4]. Here, the pressure-control mode of the hybrid DIW system was used to test the flow with various nozzle diameters and lengths. Ink was extruded through nozzles of length 13 mm and inner diameters 510, 330, 250, 150, and 100 µm. In these experiments, constant apparent wall stress values between 700 and 2200 Pa in 100 Pa increments were used across all nozzle sizes so they may be used in the Mooney analysis. Additionally, the 510 and 250 µm nozzle experiments were both repeated at nozzle lengths of 19.4 and 35 mm to conduct the Bagley [12] analysis to determine the pressure losses at the nozzle entrance. Apparent wall stress was calculated as  $\tau_{wall,apparent} = \frac{PR}{2L}$ , where R is the nozzle inner radius, L is the nozzle length, and P is the apparent pressure drop across the nozzle. This equation was used to determine the input pressures required to achieve the target apparent wall stress for each nozzle diameter and length.

The procedure followed during these experiments is as follows: After the desired pressure value was achieved within the error margin of the pressure sensor (  $\pm$  1 PSI) and the real time display of the current piston velocity multiplied by piston area (referred to as the input flow rate going forward) was stabilized as shown in Supporting information section S1.2 Fig. S7, the pressure was reset to the baseline level to retract the ink and stop flow without inducing a vacuum that would cause an air bubble in the syringe. Once the baseline pressure was reached, the next pressure was input, and a new test was started. The pressure was reset to the baseline pressure and the ink was retracted in this way between each data point. During this procedure, detection of the steady-state behavior of the input flow rate is critical as it indicates, along with the steadystate behavior of pressure, that a constant ink flow rate equal to the input flow rate is achieved. To properly detect the settling of input flow rate, the piston position data is processed with a moving linear regression approach to determine its effective rate, while reducing the influence of noise.

The input flow rate display, which was used during experiments to observe if the volume flow rate had settled, employs a linear fit on a window of 200–700 piston position vs time data points (depending on the nozzle size being used) multiplied by the piston area. The input flow rate was considered settled once its variation was limited to  $\pm$  1E-12 m³/s within a time period corresponding to more than twice the window size specified above. Exact volume flow rates that were used for further analysis were obtained by post-processing of piston position and time data once the experiment was ended. The corresponding apparent strain rate was then calculated as  $\dot{\gamma}_{apparent} = \frac{4Q}{\pi R^3}$  where Q is the average volume flow rate given by the syringe piston velocity multiplied by its area,  $Q = V_{piston} A_{piston}$  at pressure and velocity steady-state, and R is the inner radius of the nozzle. Further details pertaining to the analysis of the results of these experiments are outlined in Section 3.3 along with the corresponding results.

# 2.5. Iterative pressure control-based approach for prototyping volume flow rate control

Towards achieving precise control of the volumetric flow rate, with sufficiently short response time, we investigated the feasibility of an iterative control approach through several experiments. Here, we used the same procedure outlined in 2.4.2 where the closed-loop pressure control was adopted, but target pressure of this system was varied by the user iteratively to eventually achieve a target flow-rate level. Specifically, the largest and the smallest diameter nozzles (510 and 100  $\mu$ m) were used with the objective of achieving 1.5E-10 m<sup>3</sup>/s and 8E-12 m<sup>3</sup>/s flow rates, respectively. During the experiments, an initial pressure estimate using the rotational rheology data was used such that  $P_0$  $k(\frac{2L\tau_{max}}{r})$  where L is the nozzle length, r is the nozzle inner radius,  $\tau_{max}$  is the max shear stress recorded from the rotational rheology experiments at 20 °C after slip correction, and k is a constant selected to be 1/3. The k value was chosen so that: (1) the calculated pressure was low enough it would not exceed the pressure capacity of the syringe and the pressure sensor in the case that rotational apparent wall stresses were much lower for a given strain rate as compared to extrusion, and (2) also high enough that the material would yield and flow. After the initial pressure input had settled, input flow rate was allowed to settle according to the same criteria outlined in Section 2.4.2. Once a relatively constant input flow rate was achieved (at steady-state, input flow rate is equal to the ink flow rate), the settled flow rate was recorded, and the target pressure was adjusted to 125% the initial pressure. The pressure and input flow rate were allowed to settle, and the flow rate recorded again. A linear model was fit to these two data points and then the pressure for the final desired flow rate was calculated. The calculated final pressure was then input into the system, allowed to settle, and then the settled flow rate recorded. If the target flow rate was achieved within a certain window, then the experiment was ended. This window was dependent upon the nozzle size and target flow rate. If the target flow rate was not achieved, a quadratic fit was applied to the three pressure-flow rate points and the final pressure calculated again. This procedure was repeated with each new data point added to the quadratic fit until the calculated final pressure corresponding to the target flow rate was achieved. Further details of this implementation are presented along with the associated results in Section 3.5.

### 3. Results and discussion

### 3.1. Rotational rheometry

As noted above, the focus of rotational rheometry analysis is twofold: to understand the influence of the temperature and slip effects on the ink rheology. The temperature dependence of the ink flow behavior can be seen in Fig. 3. Flow ramps conducted in the same strain rate range and at the same gaps show that there is a lower viscosity given a higher temperature, yielding a low stress value per given strain rate. The presence of temperature dependence, even in a small temperature window, indicates that the ink behavior during DIW can vary discernibly due to small temperature variations due to regular day-to-day changes in the environmental conditions. As such, Herschel-Bulkley model fit parameters should be cast as function of temperature to be used in predictive flow rate calculations.

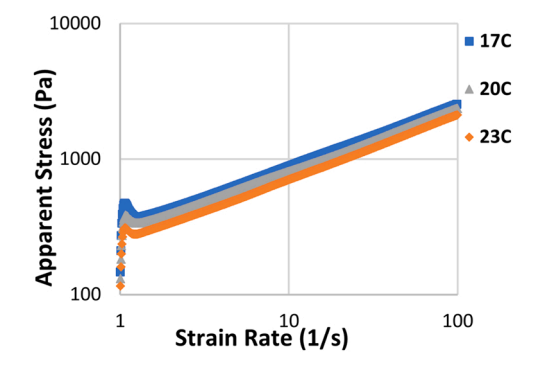


Fig. 3. Raw flow ramp data at 3 temperatures. Only 0.25 mm gap data shown for clarity.

In regard to slip behavior, Fig. 4 shows that there is a gap dependence on the stress experienced by the ink under each strain rate. This indicates that there is slip occurring between the ink and the plates as stated by the Mooney analysis (see supporting information section S1.1). In the presence of slip, a lower stress is measured for a given strain rate than if there were no slip [5]. As such, the apparent strain rate dictated by the device is less than the actual rate of strain experienced by the material, leading to the impression that the material is less viscous than it is. This error will propagate to DIW in the pressure control method, leading to erroneous predictions of the input pressure to achieve a particular flow rate. Temperature-dependent ink flow behavior can be characterized by fitting the Herschel-Bulkley models to the slip-corrected stress vs strain rate data for tested temperatures. Model parameters obtained this way are given in (Table S1 in supporting information section S1.1). Material models used in the model-based flow rate predictions discussed below were obtained through interpolating between these parameters at the room temperature measured during experimentation.

Interestingly, the model fits converged to zero yield stress at each temperature level, indicating a simpler Power-Law behavior, despite reports of this ink exhibiting yielding behavior [13]. This is likely due to the lower end of the tested strain rate range of 1–100 s<sup>-1</sup> not being low enough to capture the yield stress behavior, which is a low-strain-rate phenomenon. Nevertheless, these fits accurately capture the behavior of the ink in the apparent strain rate range relevant to ink flow inside the nozzles of interest. It should be accordingly noted that the power-law model should be considered as a mathematical representation to be used for the flow-rate prediction models detailed in Section 3.4 rather than a complete rheological representation of the ink of interest. To comprehensively understand the yielding behavior of the ink, we have conducted additional steady-shear start up rheology experiments where the ink was subjected to constant rate shear deformations for extended periods of time and shear stress was measured. We have observed that the ink exhibits both static and dynamic yielding behaviors [14-16], as evidenced by an early stress overshoot observed at high strain rates and substantially slower yielding at low strain rates [17,18]. Detailed results of these experiments are presented in the supporting formation Section S1.2. These findings are particularly relevant to the transient flow behavior of the ink. As noted above, the primary focus of the rheological analysis in this work is steady flow under high strain rates relevant to the practical applications of the DIW process. For a more in-depth discussion of the complex properties of the yield stress materials and their implications on the transient flow, reader is directed elsewhere [19-22].

### 3.2. Transient response in the velocity-controlled method

While the velocity-controlled approach, where the user prescribes a constant piston velocity, allows for direct control of the flow rate once steady flow is achieved, it can be seen from Fig. 5 that this approach suffers from an extremely long transient response when dealing with compressible inks. To objectively evaluate the transient response across

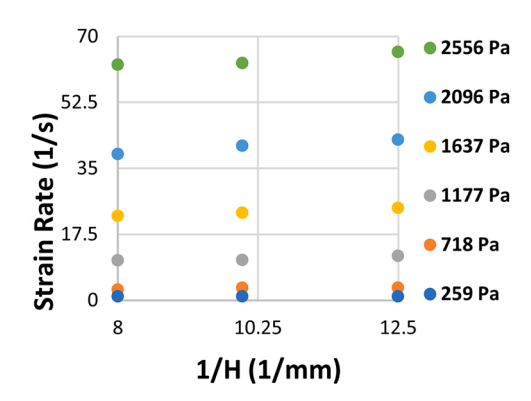


Fig. 4. Mooney Plot with only 6 stresses shown from 17 °C flow ramp.

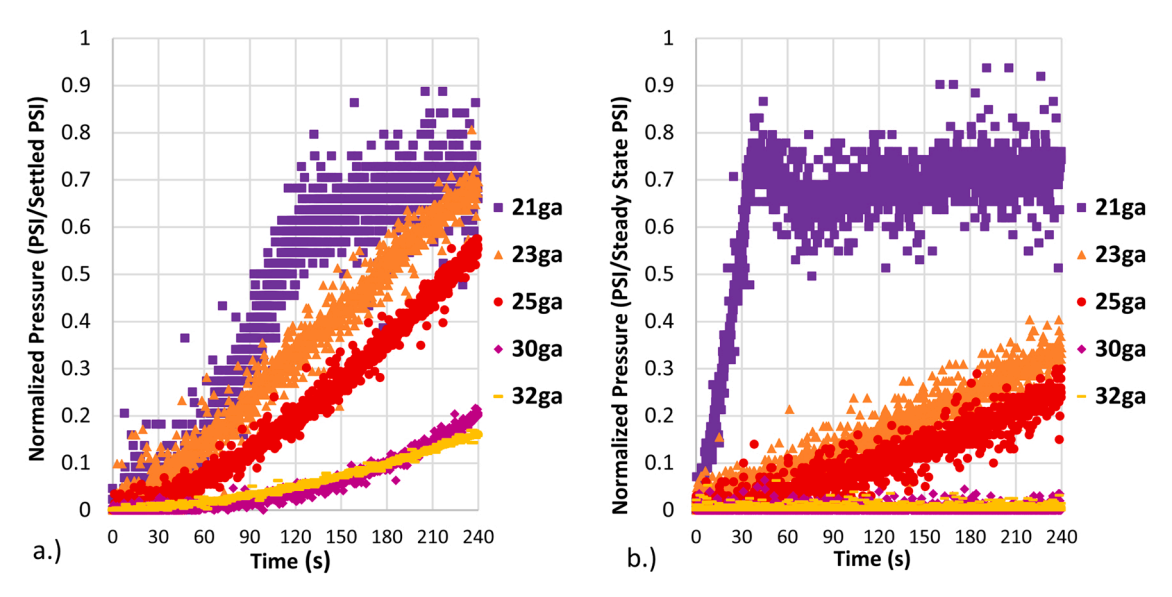


Fig. 5. Transient response of the velocity-controlled approach when there is a.) a constant piston velocity of 5E-04 mm/s across all nozzle sizes, and b.) a constant nozzle exit-velocity of 0.5 mm/s across all nozzle sizes.

different nozzle sizes, the measured pressure values have been normalized by the estimated steady-state pressure. The estimated steady state pressure per nozzle size (Table 1) was calculated by applying a quadratic fit to the flow rate and pressure data obtained through the extrusion experiments described in Section 2.4.2 (see the Supporting info section 1.2 Fig. S8 and Table S2 demonstrating the accuracy of this estimation). The Table 1 values in parentheses for 21ga are the actual steady state pressures reached during these velocity-controlled tests. This difference between predicted and observed steady state pressures for 21ga are likely due to the generally observed day-to-day variation of the ink behavior as highlighted in detail in Supporting section 1.2, specifically Fig. S9. As shown in Fig. 5, no pressures other than the 21ga case reached steady state within the 240 s timeframe. In the case of a

Table 1
Approximate steady-state pressure-velocity relations per nozzle size. Values in parentheses for 21ga are the actual steady state pressures reached during these velocity-controlled tests. All other steady-state pressure values are calculated from flow experimental data as steady-state was not reached within the given time during these tests.

Nozzle (diameter)	Steady State Pressure (PSI)	Piston Velocity (mm/s)	Flow Rate (m <sup>3</sup> /s)	App. Strain Rate (s <sup>-1</sup> )
21ga (510 μm)	15.1 (12.1)	5.00E-04	4.17E- 11	3.2
23ga (330 μm)	26.1	5.00E-04	4.17E- 11	11.8
25ga (250 μm)	40.8	5.00E-04	4.17E- 11	27.2
30ga (150 μm)	102.0	5.00E-04	4.17E- 11	125.85
32ga (100 μm)	176.0	5.00E-04	4.17E- 11	424.8
Nozzle	Steady State	Piston Velocity	Flow	App. Strain
(diameter)	Pressure (PSI)	(mm/s)	Rate (m <sup>3</sup> /s)	Rate (s <sup>-1</sup> )
21ga (510 μm)	18.8 (14.9)	1.23E-03	1.02E- 10	7.8
23ga (330 μm)	26.3	5.13E-04	4.27E- 11	12.1
25ga (250 μm)	33.5	2.95E-04	2.46E- 11	17.2
30ga (150 μm)	54.3	1.06E-04	8.83E- 12	26.64
32ga (100 μm)	75.3	4.71E-05	3.92E- 12	39.9

constant piston velocity of 0.0005 mm/s across all nozzle sizes (Fig. 5a), the pressure had only increased 10–70% towards the estimated steady-state pressure within 4 min, with the exception of the largest nozzle case (21ga) which did reach steady state. In the case of a constant exit velocity of 0.5 mm/s across all nozzle sizes (Fig. 5b), again the most significant pressure increase is seen in the largest nozzle (21ga), reaching steady-state pressure at about 30 s while the rest of the pressures went up to only 1–35% of steady-state value for the smaller nozzles, within 4 min after which the experiments were terminated. In both experiments shown in Fig. 5, the rate of pressure increase relative to the steady-state pressure decreases with decreasing nozzle diameter. This will mean a longer settling time as nozzle size decreases.

The observed transient pressure response of the inks during velocitycontrolled extrusion are likely a manifestation of the ink rheology and compressibility. To understand the contribution of ink rheology, considering the velocity (thus strain rate) controlled nature of this process, we conducted steady-shear start-up experiments, particularly close to several apparent strain rates experienced by the inks during the velocity-controlled extrusion experiments. Results of this analysis is presented in the supporting information, Fig S5. It can be observed that it takes longer than 300 s for the inks to exhibit steady shear stress, indicating that the transient ink rheology contributes to the slow settling of the pressure response during velocity-controlled extrusion. It should be noted however that the settling time for the shear stress does not seem to be a strong function of the strain rate, unlike the transient response of pressure during velocity-controlled extrusion. This could indicate that (1) compressibility effects are the major contributor to the transient pressure response and/or (2) the true strain rate, especially for the smaller nozzle diameter cases are substantially smaller than the apparent ones, due to the increased wall slip effects (elaborated upon in Section 3.3). In the latter scenario, settling of the shear stress would be significantly slower as shown in Fig S4.

In the practical implementation of the velocity-controlled approach, the problem with the initiation of the flow rates is addressed through a "priming" operation where the piston is accelerated to "compress" the ink and reach the target flow rate faster. However, without a pressure output, determining the correct priming parameters such as piston acceleration, overshoot of piston speed and deceleration for different cases would require cumbersome experimentation. Furthermore, after initiation of the flow rate, the velocity-controlled approach still presents transient response issues if the flow rate is to be varied during the prints to account for the variations of the printing speed (e.g. corners, points

where the printing direction changes) [23]. Additionally, size-scale dependent challenges faced while printing with smaller nozzles will also introduce uncertainty in the steady-state flow rate response of the velocity-controlled approach. Specifically, when printing with small nozzles, property change in the inks during extrusion due to any heterogeneity (such as low or high viscosity zones) will have a greater effect on the extrusion process due to the smaller volume of ink being extruded per unit time. It is expected that the ink pressure will fluctuate due to the rheological variations of ink flowing through the nozzles, introducing transient disturbances in the flow rate response. Since the velocity-controlled approach has a very slow transient response for small nozzles, it would also inherently respond to such disturbances in a lagging manner leading to actual flow rate fluctuations thus defeating the primary purpose of the method. Finally, the experimental iterations to determine the right priming parameters and steady-state targets best suited for a given application will take significant time. This constitutes another issue with solvent-based inks since without proper mitigation techniques, nozzle clogging is likely to occur with smaller nozzles [13] during these iterations, inducing further delays in the process.

### 3.3. Study of slip and end effects in flow behavior during ink extrusion

The raw pressures vs volume flow rate data (referred to here as flow curves) obtained during the extrusion experiments can be found in supporting information section S1.2 for each nozzle size used. As noted in Section 2.4.2, to determine the pressure loss at the nozzle entrance, the Bagley analysis and associated experiments were conducted by obtaining additional pressure vs flow rate data using nozzles of different lengths. The results of the Bagley analysis were then used to correct the apparent wall stress values corresponding to each extrusion experiment following the procedure highlighted in the literature [12]. These additional experiments for Bagley analysis had to be performed on the same day as the rest of the experiments to eliminate day-to-day variation of the ink rheology which would otherwise cause the Bagley analysis to be unapplicable to the flow curves due to a significant change in the pressure-to-volume volume flow rate relationship as seen in Fig. 6. In this procedure, once the flow curve experiments were complete, a lowand high-end volume flow rate was chosen from each of the nozzle sizes so that they could be used for the Bagley analysis [12]. Flow rates between these high- and low-end values were linearly interpolated. Details of the Bagley analysis can be found in supporting information section S1.3.

For the Mooney analysis, the Herschel-Bulkley model given in Eq. (1) was applied to each corrected wall stress vs apparent strain rate data set

to estimate the apparent strain rate for any wall-stress level, including the ones that were not experimentally tested. Flow curves for data from each nozzle that were generated using the Herschel-Bulkley fit parameters (listed in Table S3 in supporting section 1.2) are shown in Fig. 7 and used for the Mooney analysis. It should be noted that these fits are different than those presented in Section 3.1. They were used only as a mathematical fit to estimate non-tested data points and not meant as a means to characterize material rheology. The original stress range of 700–2200 Pa was used, in increments of 10 Pa, and the Mooney analysis [4] was applied to the calculated flow curve data. The detailed procedure for the capillary Mooney analysis is outlined in supporting information section S1.4.

As shown in the Mooney plot, Fig. 8, the constant slip velocity assumption (indicated by a linear increase in apparent strain rate with the reciprocal of nozzle radius) does not hold for all the nozzles sizes considered. It can be seen that for nozzles larger than 25ga (R = 0.125 mm, 1/R [1/mm] = 8) the points deviate from the line that fits the data from the smaller nozzles highlighted by the dashed blue line slope of which corresponds to four times the slip velocity ( $4v_{z,slip}$ ). The deviation from constant slip velocity for a given stress in smaller nozzles was not predictable by any current theory [8]. Several possible explanations could be provided for this behavior corresponding to the smaller nozzles as detailed below:

As shown by Wang et al. [24], there is a possibility that the polymer chains entangled at the nozzle wall are detangling under sufficient stresses and causing a two-phase slip transition behavior: stick-slip and slip-slip transitions. Before discussing these, it should be noted that while this is not directly a nozzle size-dependent phenomenon, it is

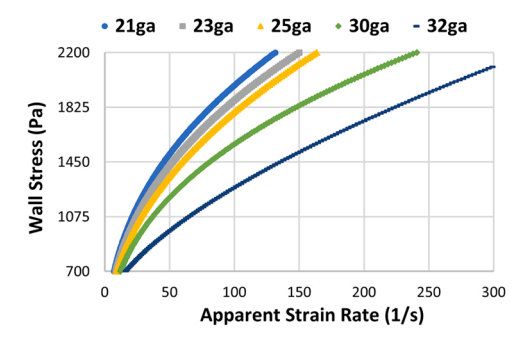


**Fig. 7.** Bagley-corrected flow curves calculated by using model parameters found in Table S3 in supporting section 1.2.

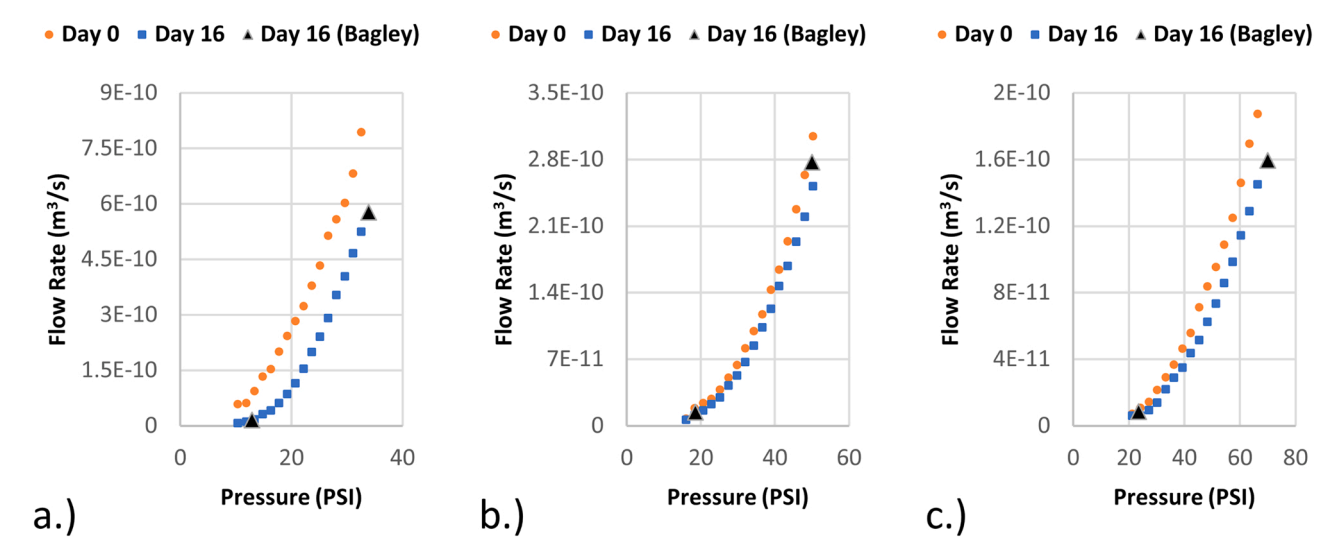


Fig. 6. Variation in flow data from multiple days for a.) 21ga (510 µm) nozzle b.) 23ga (330 µm) nozzle and c.) 25ga (250 µm) nozzle.

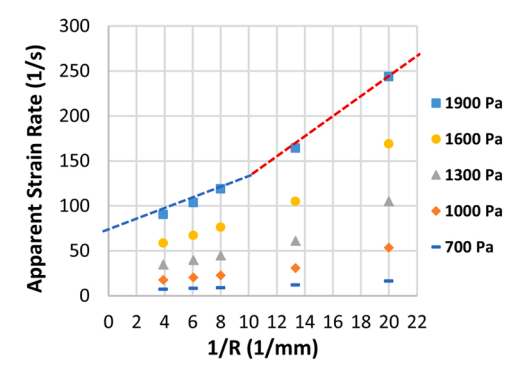
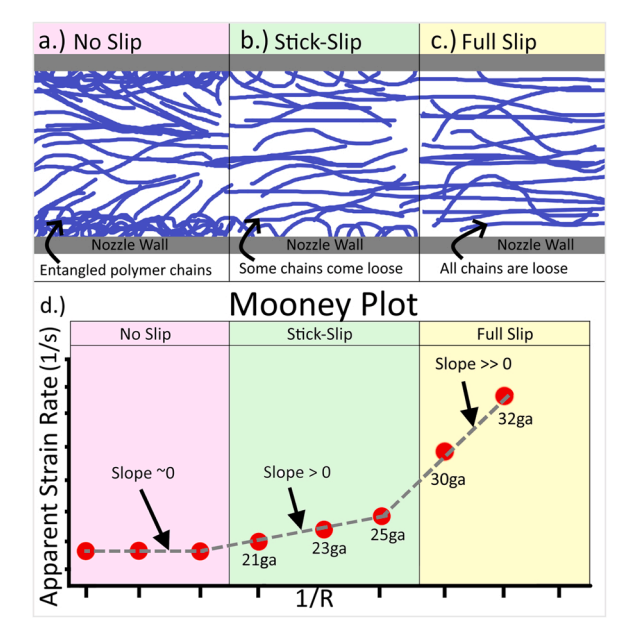


Fig. 8. Mooney Plot for extrusion experiments showing only 5 stresses.

stress-dependent, and it is known that for a given flow rate, the required stresses increase as nozzle size decreases (Fig. S12 in Supporting information section 1.3), implying a higher likelihood of the two-phase slip in smaller nozzles. The slip transitions are described as follows and illustrated in Fig. 9: At low stress levels (or in larger nozzles) the wall slip is generally negligibly small as shown in Fig. 9a. In the case of stick-slip, stresses are high enough that slip behavior starts to occur (Fig. 9b). The least entangled polymer chains are disengaging from the nozzle wall surface and sliding freely along it while the most entangled chains are still attached. Here, one could define the effective slip velocity as the average velocity of detached polymer chains at the nozzle wall. In the case of slip-slip (Fig. 9c), the stresses become high enough that even the most entangled chains detach from the nozzle wall. Now, with all polymers detached and sliding along the nozzle wall, full slip is occurring. The effective slip velocity in full-slip mode is naturally higher than the stick-slip mode due to the lack of friction from still-entangled polymer chains to hinder the flow of the detached ones along the nozzle wall. The implication of such multi-phase slip behavior on the results of the Mooney analysis is schematically described in Fig. 9d. The Mooney analysis of our extrusion experiments (Fig. 8) may accordingly suggest that the full-slip behavior is dominant for 30 and 32ga nozzles whereas the stick-slip behavior is dominant for the larger nozzles. It should also be noted that any slip effects that are dependent on polymer



**Fig. 9.** An illustration of polymers flowing through a nozzle, with a.) all polymers at nozzle wall attached to the wall, b.) some polymers detached, and c.) all polymers detached from the nozzle wall. d.) is a corresponding example Mooney plot.

chains at the nozzle wall perimeter will have a greater effect on flow rate as nozzle size decreases since the inner nozzle perimeter-to-area ratio increases in an inverse power law fashion by  $\frac{P}{A}=2(r)^{-1}$ , where P is the nozzle inner perimeter, A the nozzle opening area, and r the inner nozzle radius. As shown in Fig. 10, due to this ratio and assuming any irregular polymer behavior happening at the nozzle wall is of the same layer thickness, there will always be a greater relative effect in smaller nozzles.

The above explanation for the slip transitions is dependent on the assumption that the slopes of the Mooney plots for different nozzle diameters accurately represent the slip velocity for the corresponding cases. Another explanation could be that the standard Mooney analysis is unable to capture a more accurate picture of complex slip behavior. Since slip is not directly measured through the Mooney analysis but rather indirectly calculated from pressure and volume flow rate measurements, any measured increase in volume flow rate would lead to a higher calculated slip velocity. This is the case even if flow rate is increasing due to another reason other than increasing wall slip. A potential way this could happen is if the polymer chains align near the nozzle wall due to shear, local separation of the solvent and the polymer could occur, and an associated low viscosity zone could be formed [25, 26]. This in turn increases the shear rate at the nozzle wall, effectively increasing the volume flow rate without increasing the actual slip velocity as it is defined in the Mooney analysis. However, due to the increased flow rate, slip velocity would be calculated as a higher value than what it could be in reality. This would be more prevalent for smaller nozzles where greater alignment near the nozzle wall is expected [8]. Further, assuming the size of the low-viscosity region is only a function of ink constituents but not the nozzle size, one could suggest that the ratio of the size of low the viscosity region to that of the entire flow region is greater in smaller nozzles. This could lead to a greater contribution from this phenomenon to the increase in measured volume flow rate than in larger nozzles (Fig. 10) consistent with our experimental results.

While these theories are currently very difficult to directly verify, their potential effects on flow behavior measurement are clearly seen. Whatever the cause may be for the apparent slip velocity increase observed, it is not captured by the predictive flow rate models used to date in the DIW literature. The next section looks into the possible errors associated with that lack of sophistication of said models.

# 3.4. Comparison of predicted volume flow rates to measured volume flow rates

As stated in the introduction, the approach commonly used for prediction of flow rates for a given input pressure during DIW using cylindrical nozzles ignores the wall slip effects detailed in Section 3.3. This study was carried out to observe how closely the conventional volume flow rate prediction framework can estimate the actual flow rates

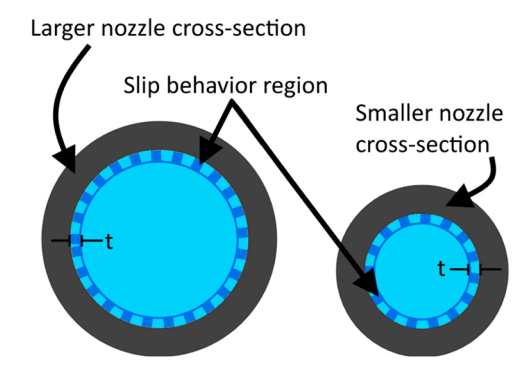


**Fig. 10.** Cross-section of large and small nozzle with slip behavior region of same thickness (t).

measured in the extrusion experiments. To this end, the Herschel-Bulkley model fits applied to the rotational rheological data were used as the material model required for this framework. For a given wall stress value, under the assumption of zero wall slip, the flow rate of a power-law fluid through a straight nozzle is given by Eq. (2) [27]:

$$Q_{theory} = \frac{n}{3n+1} \frac{\pi D^3}{8} \left(\frac{\tau_w}{k}\right)^{1/n} \tag{2}$$

where  $\tau_w$  is the shear stress at the printing nozzle wall, as given by (3):

$$\tau_{w} = \frac{D\Delta P}{4I} \tag{3}$$

where  $\Delta P$  is the pressure drop across the nozzle calculated from corrected wall stresses, L is the length of the metal portion of the nozzle, D is the nozzle diameter, and k and n are model parameters given in Eq. (1). These parameters from the rotational rheology data presented in Section 3.1 were evaluated at 20 °C, the same temperature as the volume flow rate data from extrusion experiments was gathered at.

In an effort to refine these predictions by incorporating the effect of wall slip, results from the Mooney analysis given in Section 3.3 were used to calculate the contribution of wall slip to the volume flow rate. This contribution was added on to the theoretical volume flow rates calculated using Eq. (2). The slip-corrected volume flow rate equation then becomes:

$$Q_{theory,slip} = Q_{theory} + Q_{slip} \tag{4}$$

where  $Q_{\text{slip}}$  is the volume flow rate from slip, as given by slip velocity,

 $v_{slip}$ , multiplied by the area of the nozzle opening,  $A_{nozzle}$ :

$$Q_{slip} = v_{slip} A_{nozzle} \tag{5}$$

To determine the slip velocity ( $v_{slip}$ ) for different nozzle sizes, we considered multiple approaches because of the uncertain nature of the apparent slip velocity increase presented above. For the larger three nozzles, we considered 1/4th of the slope of the lines connecting the data only for the three larger nozzles in Fig. 8. For the smaller two nozzles we adopted three possibilities: (1) we assumed the same slip velocity as the larger nozzles, (2) we considered 1/4th of the slope of the lines connecting the data from all five nozzles as the slip velocity and (3) we considered 1/4th of the slope of the lines connecting the data only for the smaller two nozzles as the slip velocity.

Errors of non-slip corrected flow rates for various nozzle sizes as a function of apparent wall stress is given in Fig. 11a, with the largest nozzle (21ga) expectedly having the lowest error (-40%) at the highest apparent wall stress and this error increasing as nozzle size decreases. All predictions are an underestimation of the flow rates measured during experimentation, as indicated by the negative error values. This underestimation is consistent with the fact that the wall slip, which effectively increases the flow rate, is not considered in this model. Further, the errors are greater for smaller nozzles because the flow rate contribution from slip relative to the overall flow rate is greater since slip velocity increases with increasing apparent wall stress (Fig. S14 in Supporting information Section S1.4). Fig. 11b shows that all errors decreased with the addition of the flow rate attributed to slip onto the theoretical prediction. The results presented in this figure corresponds to the first slip velocity calculation scheme described above which uses the

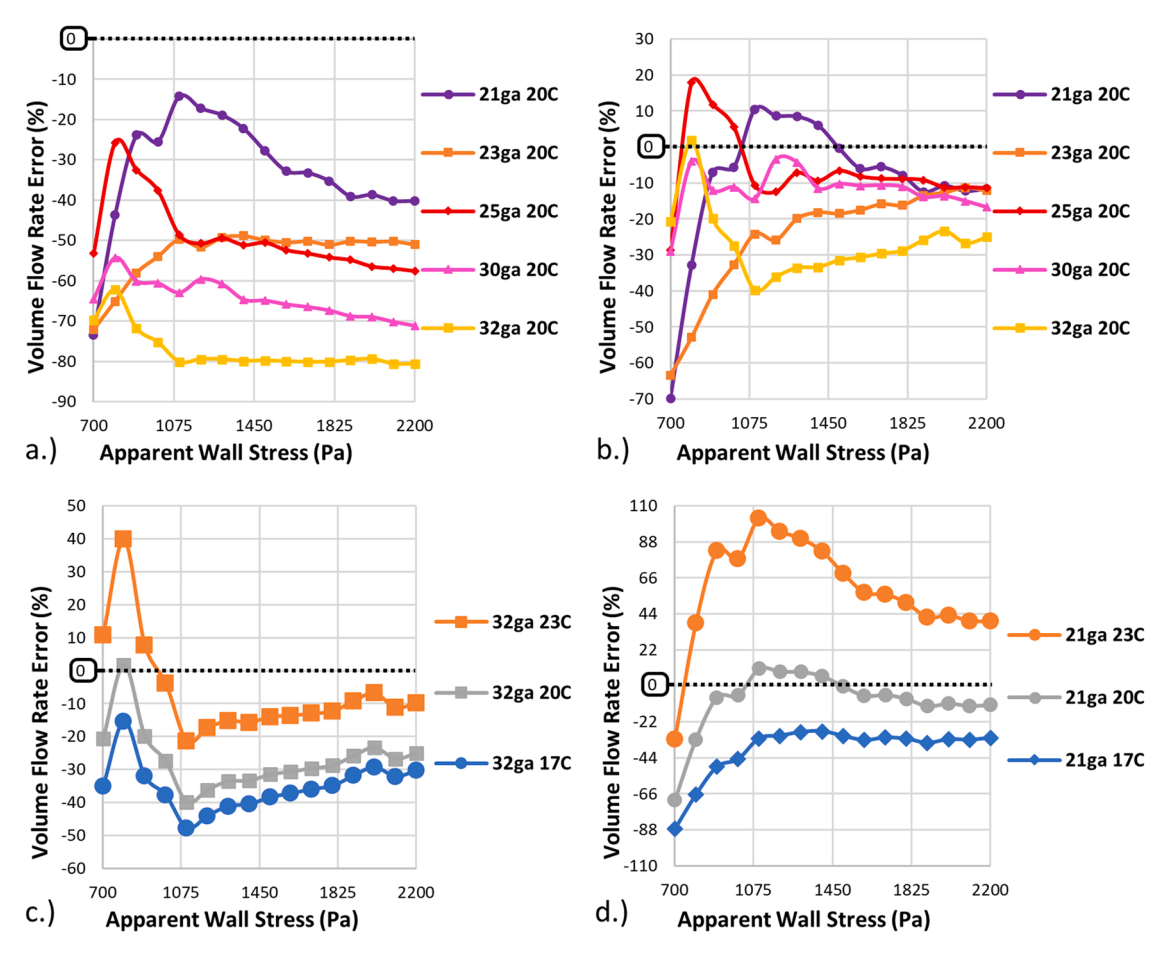


Fig. 11. Error between measured volume flow rate data and calculated volume flow rates per nozzle at a.) 20 °C, b.) 20 °C with flow rate from slip added on to calculated values, c.) 32ga nozzle size only at 17, 20, and 23 °C with flow rate from slip added, and d.) 21ga nozzle size only at 17, 20, and 23 °C with flow rate from slip added.

data from only the larger nozzles. Here, the three large nozzles have the lowest error (-11.5%, -12%, -11.4%) at the highest apparent wall stress and the smaller nozzles exhibit larger errors at the same apparent wall stress level (-16.7%, -25%). Errors were still higher for the smaller nozzles sizes even when accounting for slip, and it is likely due to the flow rate contribution from slip being calculated here using only the three largest nozzle sizes. The results obtained through the other two slip velocity calculation schemes for small nozzles are given in Fig. S15 and S16 in supporting information section S1.4. Although the errors for smaller nozzles vary depending on the choice of this scheme, there is no obvious trend that would render an optimal scheme in this case for both small nozzles.

In Fig. 11c and d, the flow rate errors when using the Power-Law parameters were calculated at not only the temperature when the extrusion experiments were carried out (20  $^{\circ}$ C) but also at 17 and 23  $^{\circ}$ C. This shows it is important that the temperature at which rheometry is performed matches the temperature at which extrusion experiments are performed for prediction accuracy. Further, in the case of small nozzles such as the 32ga size, the accuracy of predictive models is so low that using predictive parameters from an incorrect temperature such as 23 °C instead of 20 °C yields a more accurate prediction as a rheological coincidence. This is due mostly to the fact that slip during extrusion causes the model to under predict flow rates while the highertemperature parameters compensate for this because an ink exhibits lower viscosity at higher temperatures. This is not the case for larger nozzles such as 21ga as shown in Fig. 11d, where using the correct parameters calculated at 20 °C still yields the most accurate prediction because slip effects are not as dominant. For all cases, however, challenges with predictive models are compounded further because of the high day-to-day fluctuation seen between volume flow rates given the same input pressure, nozzle size, and ink. This means a prediction may

be more or less accurate depending on the day and any other uncontrollable ambient variables (Fig. 6). Finally, another potential contributor to the prediction error particularly at lower stresses and thus lower pressure levels could be the uncertainty as to whether the "steady-state" was achieved during the experimentation. This is expected since the transient response of the system is significantly slower at low flow rate levels.

### 3.5. Iterative pressure control for prototyping volume flow rate control

To evaluate the performance of the proposed iterative pressure control approach in achieving target flow rate values with improved transient response compared to the traditional velocity-controlled approach, we performed two benchmark tests in velocity-controlled mode using the largest and smallest (21ga and 32ga) nozzles and measured the baseline settling time for each case. In these experiments target flow rates of 1.5E-10  $\rm m^3/s$  and 8E-12  $\rm m^3/s$  were used for the 21ga and 32ga nozzles, respectively. Here, the system was deemed to reach the target flow rate once the measured pressure reaches a steady-state. Fig. 12a and b show transient response recorded during these experiments. The response is expectedly much quicker for the larger 21ga nozzle (steady state in  $\sim\!80~\rm s$ ) versus the smaller 32ga nozzles (steady state in  $\sim\!2200~\rm s$ ).

As noted in Section 2.5, the pressure control was activated with the initial pressure selected as  $P_0 = \frac{1}{3} \left(\frac{2L\tau_{max}}{r}\right)$  where L is the nozzle length, r is the nozzle inner radius, and  $\tau_{max}$  is the max shear stress recorded from the rotational rheology experiments at 20 °C. The initial pressure was allowed to settle, and the input flow rate was observed. The input flow rate has a very large value at first as the piston is moving very quickly to pressurize the system. Once the piston had slowed as indicated by the input flow rate leveling out and becoming fairly constant, the initial

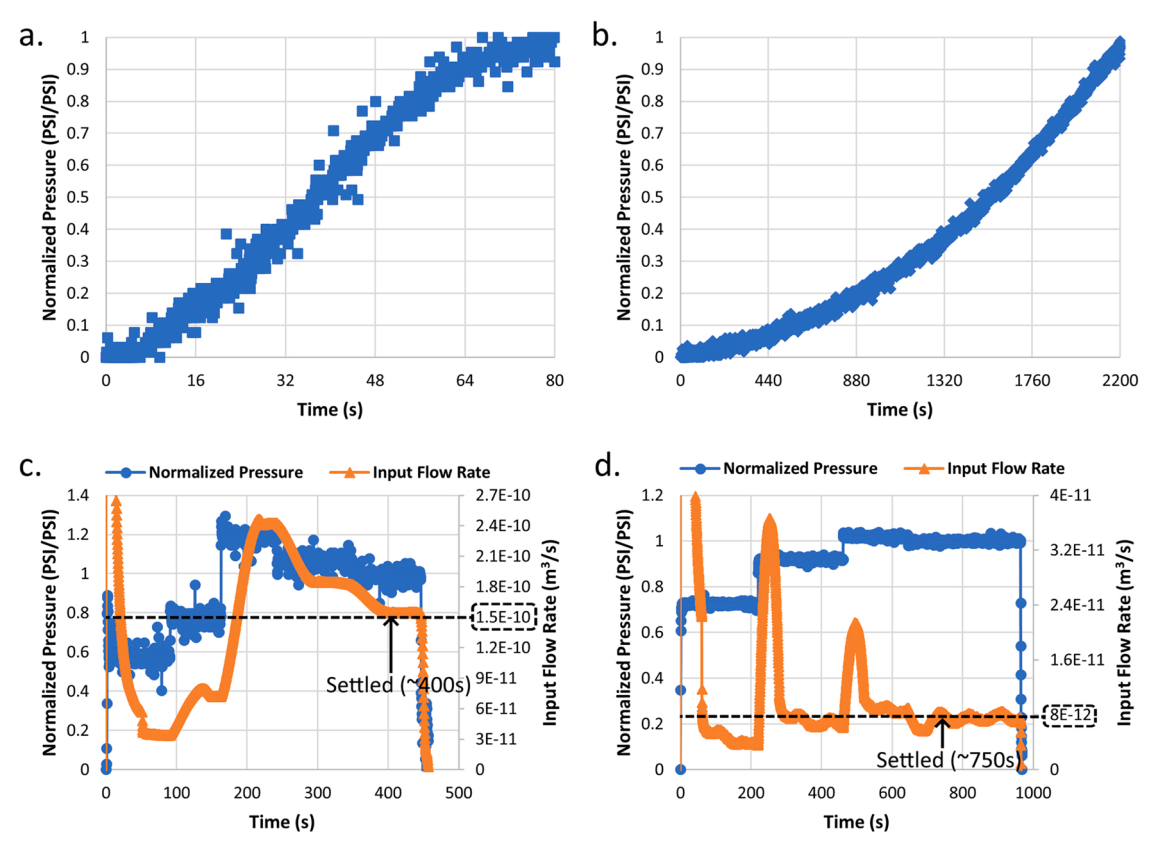


Fig. 12. Normalized pressure response of velocity-controlled system for a.) 21ga nozzle size at 1.8E-3 mm/s piston speed, and b.) 32ga nozzle size at 9.6E-5 mm/s. Pressure response of the PD pressure-controlled system for c.) 21ga and d.) 32ga nozzle sizes with target flow rates corresponding to input piston velocity during velocity-controlled tests.

settling was complete. Now, the input flow rate was observed for 20-60 s for the 21ga nozzle and 100-200 s for the 32ga nozzle to manually determine the average value it had settled on. If the input flow rate was outside a  $\pm$  1E-12 m<sup>3</sup>/s window around the target flow rate within that time, then the average flow rate was calculated and the experiment advanced. After the average input flow rate had been recorded, the pressure was increased by 25% and the system allowed to settle again. The first two points were now recorded and used to calculate the pressure corresponding to the target volume flow rate using a linear fit. The calculated pressure was input into the system and the piston would again move quickly after the pressure change. The pressure and piston speed were allowed to settle again as indicated by the input flow rate averaging around a new value. If the target flow rate was achieved then the experiment was ended, but if not then the process was repeated with a quadratic fit between points until the input flow rate was oscillating around the target flow rate at steady-state pressure. See Supporting Information Section S1.5 for details on quadratic fits.

When the pressure control is turned on, it can be seen in Fig. 12c and d that the size of the nozzle and corresponding flow rates has an impact on how the system responds to pressure changes when iterating for a desired volume flow rate. For 21ga, Fig. 12c shows a shorter piston velocity response time between pressure changes as compared to 32ga in Fig. 12d, and the input flow rate finally fluctuating around the target volume flow rate much sooner than in the 32ga case (~400 s for 21ga and  $\sim$ 750 s for 32ga). In comparison, it can also be seen that the velocity overshoot by the system when a pressure change is imposed is much larger relative to the target volume flow rate for the smaller nozzle, resulting in a longer settling of the overshoot. For example, the first overshoot in Fig. 12c lasts about 60 s, while the first in the 32ga case lasts about 100 s. The input flow rate fluctuations around the target flow rate are about  $\pm$  1E-12 m<sup>3</sup>/s, which is two orders of magnitude less than the absolute target flow rate for 21ga but the same order of magnitude as the 32ga target flow rate. This means the user must wait longer to determine that the input flow rate has settled at the desired value since the fluctuations are much larger relatively. It is evident that the transient behavior of the flow rate upon the pressure change is the main factor determining how fast the target flow rate can be achieved. As noted above for the velocity-controlled approach, one could expect both the ink rheology and compressibility to contribute to the transient response. To understand the influence of ink rheology in this pressure-controlled (thus constant stress) process, we conducted parallel-plate creep experiments when the ink was subjected to several levels of constant shear stresses and strain rate evolution was monitored. The results of these experiments were presented in detail in the supporting information section S1.3. It was observed that the material experiences delayed yielding as shown in Fig S6, particularly at lower stress levels that are higher than yield stress, which can be a partial contributor to the transient flow rate response. In the iterative pressure control experiments presented above, the final apparent shear stress for the 21 and 32ga nozzles were 1365 and 1228 Pa, respectively. According to our experience, after a proper Bagley correction, it is expected that the net shear stress experienced in the 32ga would be higher than 21ga. The fact that slower transient response is observed for 32ga nozzles despite the expected faster yielding may be taken as an indication that the compressibility effects are the dominant factor dictating the flow rate response.

In the case of the 21ga nozzle, steady state at the target flow rate was achieved faster using velocity control as compared to the iterative pressure control approach. This is likely the case for most large nozzles especially at higher target flow rates since the pressure increase per unit time is proportional to the piston velocity (Fig. 5a). It is clear that the iterative pressure control approach is more efficient at reaching steady state for a desired flow rate when dealing with smaller nozzles.

### 4. Concluding remarks

### 4.1. Key conclusions regarding the influence of size scale in DIW processes

In this paper, an in-depth study of the flow of yield-pseudoplastic inks during the DIW process with various nozzle sizes is presented. To this end, key factors such as temperature-dependent ink rheology, wall slip during ink extrusion, and ink compressibility are considered. Further, how these factors influence ink flow rate accuracy and transient response in conjunction with the nozzle size is investigated for both velocity and pressure control approaches. To facilitate these investigations, a novel DIW printhead implementation is introduced where ink flow rate and pressure can be simultaneously monitored. Our studies generally indicated that there is an increased level of complexity of DIW with smaller nozzles and associated challenges with controlling ink flow rate. Particularly for the velocity-controlled approach where the flow rate is directly dictated, smaller nozzles exhibited significantly slower transient response. For the pressure-control approach, where the flow rate is indirectly dictated through pressure, flow rate-pressure relationships are significantly more difficult to predict when small nozzles are involved. Specifically, due to the prominence and complexity of the wall-slip observed inside small nozzles, prediction of steady-state ink flow rate for a given input pressure require not only a thorough understanding of ink rheology, but also the interaction between the ink and the nozzle walls. Furthermore, transient behavior of the ink flow in any method is significantly more complex for smaller nozzles due to complex ink yielding phenomena and compressibility dynamics.

These results clearly layout the influence of size scale in DIW processes, indicating that different practical considerations are required at the lower extremes of the DIW size scales. One could accordingly conclude with increasing nozzle size, the feasibility of conventional DIW methods increases. Namely, for large nozzles approaching mm scales, accurate flow rates can be directly achieved with reasonable transient response using the velocity-controlled approach. Furthermore, the pressure-flow rate relationships can be accurately predicted through shear flow assumption in the pressure-controlled approach, enabling fundamental studies of flow mechanisms. For smaller nozzles in the low-hundred-micron diameter ranges, these capabilities are not achievable, making it nearly impossible to get high quality micro-scale 3D prints harboring acceptable accuracy. Addressing these limitations of micro-DIW requires new printhead and process implementations.

The iterative implementation presented in this paper can be viewed as a preliminary candidate to realize high accuracy micro-DIW. As detailed above, this approach can be viewed either as a multi-step iterative version of the pressure control method where the target pressure is varied according to the flow rate measurements, or a smart priming approach for the velocity-control method, informed through the real-time pressure input. Our results show that, from any perspective, the proposed approach achieves improved accuracy and transient performance for smaller nozzles. It should be noted that this improvement is achieved without significant effort in optimizing the pressure controller or the iteration algorithm. This indicates that the general approach of incorporating both flow rate and pressure input in a closed-loop scheme is an effective one towards realizing high accuracy flow during micro-DIW.

### 4.2. Outlook

One of the key limitations of the presented studies is that they focus only on NaCMC solutions as the ink material. This ink composition and general properties are representative of polymeric bioinks widely used in DIW applications. Many other functional inks include micro and nano-scale solid fillers and exhibit more complex rheological properties. Accordingly, one would expect even more complex size dependent behavior when these inks are involved [8]. As such, similar studies must be conducted for highly loaded composite inks to elucidate such

### complexities.

It should be noted that this study focuses on the accuracy of flow rate, which is foundational to the overall DIW process accuracy but is not the sole factor determining it. The shape evolution of the deposited ink filament under the influence of ink rheology, ink-nozzle and ink-surface interactions, and thermal or drying-based shrinkage effects also contribute to the final printed dimensions and their accuracy. It is also likely that size effects would generate fundamental differences in behavior which warrant further studies.

For the proposed control scheme, there are several aspects that require further research and development. Firstly, the closed-loop pressure-control used in each iteration currently relies on a simple PD controller. More advanced controller designs may further improve the transient response allowing quicker settling of the flow rate in each iteration. Secondly, in the current implementation, the sensing of steady-state is determined rather subjectively by the user. For robust implementation, algorithms for steady-state sensing or prediction using the transient data should be implemented. The primary challenge in such implementations would be the presence of complex system dynamics leading to multi-frequency oscillations and noise. These complexities would be variable as a function of ink properties, which adds to the associated research challenge. Finally, smarter, learning-based algorithms should be developed for iteration of target pressure values to reduce the overall transient period. Such algorithms should be compatible with various inks, thus, they could be informed through the rheological ink characterization as well as previous iteration information from the same or similar inks. Emerging machine learning approaches can facilitate development of such dynamically evolving algorithms. Furthermore, the iteration data produced during such implementations can elucidate capillary flow characteristics of various inks as well as complex relationships between such characteristics and ink compositions, offering significant research value for DIW technologies. Advances realized through successful implementation of closedloop, high accuracy micro-DIW can enable more accurate and repeatable fabrication of devices and their effective miniaturization. This is critical particularly for biomedical technologies such as artificial tissue engineering where feature resolution is key to the success of the produced structures.

Finally, it should be acknowledged that precise control of flow rate during DIW is not sufficient to fabricate structures with desired properties. This advancement requires a thorough understanding of how the inks flow and deform during DIW, leading to various microstructures achieved in the printed parts. This in turn calls for detailed rheological examination of the ink yielding and flow behavior, providing opportunities for complimenting flow-rate control approaches with capabilities to control such complex flow mechanisms.

### **Funding Statement**

This work was financially supported by the National Science Foundation (NSF) grant 1825872 and NSF Graduate Research Fellowship Award 1842493.

### CRediT authorship contribution statement

**Kevin T Estelle:** Writing – review & editing, Writing – original draft, Visualization, Methodology, Investigation, Formal analysis, Data curation. **B. Arda Gozen:** Writing – review & editing, Validation, Supervision, Project administration, Methodology, Funding acquisition, Formal analysis, Conceptualization.

### **Declaration of Competing Interest**

The authors declare that they have no known competing financial interests or personal relationships that could have appeared to influence the work reported in this paper.

### **Data Availability**

Data will be made available on request.

### Acknowledgements

The authors would like to acknowledge the help of Ruchira Tandel for help designing and constructing the hybrid extrusion system.

### Appendix A. Supporting information

Supplementary data associated with this article can be found in the online version at doi:10.1016/j.addma.2022.103183.

### References

- A.B. Dababneh, I.T. Ozbolat, Bioprinting technology: a current state-of-the-art review, J. Manuf. Sci. Eng. Trans. ASME 136 (2014), https://doi.org/10.1115/ 1.4028512
- [2] Z. Hou, H. Lu, Y. Li, L. Yang, Y. Gao, Direct ink writing of materials for electronics-related applications: a mini review, Front Mater. 8 (2021), https://doi.org/ 10.3389/fmats.2021.647229.
- [3] I.T. Ozbolat, M. Hospodiuk, Current advances and future perspectives in extrusionbased bioprinting, Biomaterials 76 (2016) 321–343, https://doi.org/10.1016/j. biomaterials.2015.10.076.
- [4] M. Mooney, Explicit formulas for slip and fluidity, J. Rheol. (N.Y.,N.Y.) 2 (1931) 210–222, https://doi.org/10.1122/1.2116364.
- [5] A. Yoshimura, R.K. Prud homme, Wall slip corrections for couette and parallel disk viscometers, J. Rheol. (N.Y.,N.Y.) 32 (1988) 53–67, https://doi.org/10.1122/ 1.549963
- [6] X.B. Chen, M.G. Li, H. Ke, Modeling of the flow rate in the dispensing-based process for fabricating tissue scaffolds, J. Manuf. Sci. Eng., Trans. ASME 130 (2008) 0210031–0210037, https://doi.org/10.1115/1.2789725.
- [7] A.A. Adib, D.J. Hoelzle, Hybrid control of flowrate in microextrusion-based directwrite additive manufacturing, IEEE Control Syst. Lett. 6 (2022) 97–102, https://doi.org/10.1109/LCSYS.2021.3049897.
- [8] P. Wilms, J. Wieringa, T. Blijdenstein, K. van Malssen, J. Hinrichs, R. Kohlus, On the difficulty of determining the apparent wall slip of highly concentrated suspensions in pressure driven flows: the accuracy of indirect methods and best practice, J. Nonnewton Fluid Mech. 299 (2022), https://doi.org/10.1016/j. innfm.2021.104694
- [9] P. Deng, J. Zhang, F. Liu, K. Liu, H. Liu, L. Zhang, Shear-induced flow behavior of three polymers in different size dies, J. Macromol. Sci. Part B: Phys. 52 (2013) 651–661, https://doi.org/10.1080/00222348.2012.720171.
- [10] A. Simeunović, D.J. Hoelzle, Nonlinear and linearized gray box models of direct-write printing dynamics, Rapid Prototyp. J. 26 (2020) 1665–1676, https://doi.org/10.1108/RPJ-12-2018-0303
- [11] H.S. Tang, D.M. Kalyon, Estimation of the parameters of Herschel-Bulkley fluid under wall slip using a combination of capillary and squeeze flow viscometers, Rheol. Acta 43 (2004) 80–88, https://doi.org/10.1007/s00397-003-0322-y.
- [12] E.B. Bagley, End corrections in the capillary flow of polyethylene, J. Appl. Phys. 28 (1957) 624–627, https://doi.org/10.1063/1.1722814.
- [13] K.T. Estelle, B.Arda Gozen, Humidity-controlled direct ink writing for micro-additive manufacturing with water-based inks, J. Manuf. Process 69 (2021) 583–592, https://doi.org/10.1016/j.jmapro.2021.07.059.
- [14] Y. Qian, S. Kawashima, Distinguishing dynamic and static yield stress of fresh cement mortars through thixotropy, Cem. Concr. Compos. 86 (2018) 288–296, https://doi.org/10.1016/j.cemconcomp.2017.11.019.
- [15] B. Zakani, D. Grecov, Yield stress analysis of cellulose nanocrystalline gels, Cellulose 27 (2020) 9337–9353, https://doi.org/10.1007/s10570-020-03429-7.
- [16] P. Coussot, Q.D. Nguyen, H.T. Huynh, D. Bonn, Viscosity bifurcation in thixotropic, yielding fluids, J. Rheol. (N. Y N. Y) 46 (2002) 573–589, https://doi.org/10.1122/11459447
- [17] K. Kamani, G.J. Donley, S.A. Rogers, Unification of the rheological physics of yield stress fluids, Phys. Rev. Lett. 126 (2021), 218002, https://doi.org/10.1103/ PhysRevLett.126.218002.
- [18] P. Coussot, Slow flows of yield stress fluids: yielding liquids or flowing solids, Rheol. Acta 57 (2018), https://doi.org/10.1007/s00397-017-1055-7.
- [19] P. Coussot, Yield stress fluid flows: a review of experimental data, J. Nonnewton Fluid Mech. 211 (2014) 31–49, https://doi.org/10.1016/j.jnnfm.2014.05.006.
- [20] E. N'Gouamba, J. Goyon, P. Coussot, Elastoplastic behavior of yield stress fluids, Phys. Rev. Fluids 4 (2019) 1–18, https://doi.org/10.1103/ PhysRevFluids.4.123301.
- [21] P. Coussot, L. Tocquer, C. Lanos, G. Ovarlez, Macroscopic vs. local rheology of yield stress fluids, J. Nonnewton Fluid Mech. 158 (2009) 85–90, https://doi.org/ 10.1016/j.jnnfm.2008.08.003.
- [22] P. Coussot, Q.D. Nguyen, H.T. Huynh, D. Bonn, Avalanche behavior in yield stress fluids, Phys. Rev. Lett. 88 (2002) 1755011–1755014, https://doi.org/10.1103/ PhysRevLett.88.175501.
- [23] R. Comminal, M.P. Serdeczny, D.B. Pedersen, J. Spangenberg, Motion planning and numerical simulation of material deposition at corners in extrusion additive

- manufacturing, Addit. Manuf. 29 (2019), https://doi.org/10.1016/j.
- [24] S.-Q. Wang, P.A. Drda, Q.S. Wang, R.A. Drda, Stick-slip transition in capillary flow of linear polyethylene: 3. Surface conditions, 1997.
- [25] C.J.R. Verbeek, L.E. van den Berg, Extrusion processing and properties of protein-based thermoplastics, Macromol. Mater. Eng. 295 (2010) 10–21, https://doi.org/10.1002/mame.200900167.
- [26] T. Guo, J.P. Ringel, C.G. Lim, L.G. Bracaglia, M. Noshin, H.B. Baker, D.A. Powell, J. P. Fisher, Three dimensional extrusion printing induces polymer molecule alignment and cell organization within engineered cartilage, J. Biomed. Mater. Res. A 106 (2018) 2190–2199, https://doi.org/10.1002/jbm.a.36426.
- [27] R.P. Chhabra, J.F. John, F. Richardson, Non-Newtonian Flow in the Process Industries: Fundamentals and Engineering Applications, Butterworth-Heinemann, 1999